Inorganica Chimica Acta 362 (2009) 1428–1434

Contents lists available at ScienceDirect

Inorganica Chimica Acta

journal homepage: www.elsevier.com/locate/ica

Syntheses, structures and magnetic properties of zig-zag chains of transition metals with O–P–O bridges

Yusuke Yoshida [a,b], Katsuya Inoue [b], Natalie Kyritsakas [a], Mohamedally Kurmoo [a,*]

[a] Laboratoire de Chimie de Coordination Organique, CNRS-UMR7140, Université Louis Pasteur, Institut Le Bel, 4 rue Blaise Pascal, 67000 Strasbourg Cedex 01, France
[b] Department of Chemistry and Institute for Advanced Materials Research, Hiroshima University, Kagamiyama, Higashi-Hiroshima 739-8526, Japan

ARTICLE INFO

Article history:
Received 28 February 2008
Accepted 2 July 2008
Available online 12 August 2008

Keywords:
Pyrophosphite
Magnetic properties
Zig-zag chain

ABSTRACT

A novel series of linear chain coordination polymers, $[NH_4][M^{II}(H_2PO_2)_3(H_2O)]$ where M = Mn, Co, Ni, has been obtained by the reaction of divalent metals salts with ammonium pyrophosphite, $[NH_4][H_2PO_2]$, in a methanol–water mixture. They crystallise in the monoclinic $P2_1/n$ cell and contain polar chains aligned with opposing polarity. Both bridging and terminal monodentate coordination modes are exhibited by the $H_2PO_2^-$. Two types of hydrogen-bond between a coordinated water and a monodentate $H_2PO_2^-$ connect the chains into a 3D-network. The compounds have been further characterised by IR and UV–Vis spectroscopies, TGA, and their magnetic properties measured. All three compounds exhibit weak antiferromagnetic nearest neighbour interaction. A similar study on the known $[Fe^{III}(H_2PO_2)_3]$ is also reported. Its magnetic susceptibility fits a model for a 1D-antiferromagnet with 2 J/*k* of 1.20(1) K and *g* of 2.019(2).

1. Introduction

In developing magnetic materials, chemists have for a number of years been interested in coordination polymers of transition metals [1,2]. Among the criteria for obtaining long-range magnetic ordering, the number of bridging atoms between the moment carriers is an important factor as it defines the strength of the magnetic exchange interaction between the nearest-neighbour moment carriers [3]. The strength decreases with the number of bridging atoms in the connector; for example the critical transition temperature, being dependent of the exchange interaction, is above 800 K for the oxides (one-atom bridge) and decreases to nearly 200 K for the Prussian blue family having two-atom cyanide bridges while for those containing three-atom, T_C are less than 30 K [4]. There is considerable interest by magneto-chemists in using three-atom bridges due to the wider range of chemicals available and only few systems are known where every metal centre is bridged uniformly [5]. Amongst them are those containing azide [6], imidazole [7], dicyanamide [8], carbonate [9], oxalate [10] and formate [11]. The latter has been of much importance to us in the development of materials exhibiting dual property, such as porosity and magnetism [11]. Following this line of work, we are searching for other ligands to mimic the formate ion and therefore, we have started a study of the structural and magnetic properties of hypophosphite, $H_2PO_2^-$, complexes of transition metals.

Hypophosphite salts are known for metals of the alkali [12], alkaline earth [13], transition [14–18], lanthanide [19], and group 14 [20]. Several examples of organic cations are also known to form stable salts. Coordination complexes with a third component, a coordinating organic ligand such as urea, phenanthroline or bipyridine, are known for copper and manganese [21]. Among them, several coordination complexes have been isolated with paramagnetic cations of the first row transition metals. Only few studies of their magnetic properties have been performed and the results show that only two of them exhibit long-range magnetic ordering; $CoCl(H_2PO_2)\cdot H_2O$ is a weak ferromagnet below 8.4 K but $NiCl(H_2PO_2)\cdot H_2O$ is a Curie–Weiss paramagnet above 4.5 K and $Mn(H_2PO_2)_2\cdot H_2O$ is an antiferromagnet below 6.5 K [14,16].

Interestingly, the copper(II) complex, $Cu(H_2PO_2)_2$, is not very stable and it displays two consecutive phase transitions transforming it between the three ground states [17]. Also of current interest is the variable water content of the cobalt complex, $Co(H_2PO_2)\cdot xH_2O$, x = 0–0.69, which is obtained from cobalt sulfate and it adopts a layered structure where the amount of water residing in the gallery can be altered or replaced by a mixture of pyridine and water (1.86 py and 0.31 H_2O) [14].

Here, we report the syntheses, single-crystal structure determinations, thermogravimetric analyses, optical spectroscopy and the magnetic properties of an isostructural series, $[NH_4][M^{II}(H_2PO_2)_3(H_2O)]$, where M = Mn (**1**), Co (**2**) and Ni (**3**) as well as those of the structurally characterised $[Fe^{III}(H_2PO_2)_3]$ (**4**) [18].

* Corresponding author. Fax: +33 390241356.
E-mail address: kurmoo@chimie.u-strasbg.fr (M. Kurmoo).

0020-1693/$ - see front matter © 2008 Elsevier B.V. All rights reserved.
doi:10.1016/j.ica.2008.07.009

2. Experimental

2.1. Synthesis

$[NH_4][H_2PO_2]$: 158 mL of 50% H_3PO_2 ($d \sim 1.274$ g/cm^3, 1.58 mol) was mixed slowly to 130 mL of 26% aqueous ammonia solution ($d \sim 0.90$ g/cm^3, 1.72 mol) and the mixture was evaporated to yield a white powder. It was dissolved into 150 mL of hot methanol and the solution was cooled before 300 mL of ether was added while stirring. A white crystalline precipitation was obtained after a few hours followed by filtering and washing with ether and finally dried in vacuum. Yield 104.4 g, 82.3%.

$[NH_4][Mn^{II}(H_2PO_2)_3(H_2O)]$ (**1**): A mixture of 2.6 mL of 1.0 M $[NH_4][H_2PO_2]$ in CH_3OH, 0.3 ml of 1.0 M $MnCl_2 \cdot 4H_2O$ in CH_3OH and 1.1 mL of water was placed at the bottom of a glass tube. The mixture was then layered with 8 mL of acetone, capped and left to stand. After one week pale pink needle crystals of **1** and few clear pink blocks of $[Mn^{II}(H_2PO_2)_2(H_2O)]$ were harvested. The crystals were separated manually under an optical microscope for further measurements. Yield 63.7 mg, 74.3%. *Anal.* Calc.: H, 4.23; N, 4.90. Found: H, 3.83; N, 4.90%.

$[NH_4][Co^{II}(H_2PO_2)_3(H_2O)]$ (**2**): A mixture of 0.3 mL of 0.4 M $CoCl_2 \cdot 6H_2O$ in CH_3OH, 2.4 mL of 1.0 M $[NH_4][H_2PO_2]$ in CH_3OH, 1.2 mL of water was placed in a glass tube and left open to air. After 1 week the mixed solution had concentrated and hexagonal purple-red plate crystals were harvested. Yield 71.0 mg, 61.2%. *Anal.* Calc.: H, 4.17; N, 4.83. Found: H, 3.93; N, 4.98%.

$[NH_4][Ni^{II}(H_2PO_2)_3(H_2O)]$ (**3**): A mixture of 1.0 mL of 1.0 M $NiCl_2 \cdot 6H_2O$ in CH_3OH and 5.0 mL of 1.0 M $[NH_4][H_2PO_2]$ in CH_3OH was placed in a glass tube and left open to air. The crystals are formed in two steps; first green blocks are formed which over a period of one week turned into hexagonal yellow-green plate crystals of the desired compound. The crystals were harvested and washed with ethanol and acetone. Yield 227 mg, 78.2%; *Anal.* Calc.: H, 4.18; N, 4.84. Found: H, 3.64; N, 4.78%.

$[Fe^{III}(H_2PO_2)_3]$ (**4**): 270 mg (4.83 mmol) of Fe powder in a small glass tube (φ5 mm, 35 mm height) was placed at the bottom of a large glass tube (φ14 mm). 10 mL of 50% H_3PO_2 (96.5 mmol) was then added to cover the small tube. After two months, colourless crystals were harvested. The small tube with the remaining Fe powder was taken out and the products in the large glass tube were collected. Yield 1.743 g, 48.1%.

$[Co^{II}(H_2O)_6](H_2PO_2)_2$ (**5**): 2 mL of an aqueous solution containing 4.0 M $[NH_4][H_2PO_2]$ and 1.0 M $CoCl_2 \cdot 6H_2O$ was placed at the bottom of a glass tube. The solution was the layered with 8 mL of acetone and left. After 5 days, the red crystals formed were collected. Yield 0.432 g, 72.5%. The crystals were distinctly different in shape and colour from those of **2**. This phase was checked by determination of the unit cell on single crystal [14].

2.2. Characterization

Powder X-ray diffraction patterns were recorded using either a Rigaku Rint 2000 system equipped with Cu Kα radiation or a Siemens D500 equipped with Co Kα radiation and employing a scan rate of 4°/min and scan step of 0.02°. The simulated patterns were calculated from single crystal X-ray data using RIETAN-2000 program [22].

For the single-crystal X-ray structure determinations, diffraction intensity data at 173 K were collected for selected crystals mounted on glass fibres using a Bruker SMART Apex CCD diffractometer equipped with Mo Kα1 radiation. Absorption corrections were applied using the multiscan program SADABS [23]. The structures were solved by direct methods, and the non-hydrogen atoms were refined anisotropically by the least-squares method on F^2 using the SHELXTL program [24]. The hydrogen atoms were either found by difference Fourier maps or were generated geometrically at theoretical positions using the riding model (C–H, 0.96 Å, N–H, 0.90 Å). Crystal data, as well as details of the data collection and refinement, for the complexes are summarised in Table 1.

Table 1
Crystallographic data for $[NH_4]$ $[M^{II}(H_2O)(H_2PO_2)_3]$

Compound	**1**	**2**	**3**
Formula	$H_{12}MnNO_7P_3$	$H_{12}CoNO_7P_3$	$H_{12}NiNO_7P_3$
F_w	285.96	289.95	289.73
T (K)	173	173	173
Atmosphere	nitrogen	nitrogen	nitrogen
Crystal System	monoclinic	monoclinic	monoclinic
Space group	$P2_1/n$	$P2_1/n$	$P2_1/n$
a (Å)	7.4412(6)	7.3669(15)	7.3202(2)
b (Å)	15.1467(12)	14.914(3)	14.7961(4)
c (Å)	9.3051(5)	9.2048(18)	9.1762(2)
β (°)	108.230(2)	108.38(3)	108.8140(10)
V (Å^3)	996.13(12)	959.7(4)	940.78(4)
Z	4	4	4
D_C (g/cm^3)	1.907	2.007	2.046
μ(Mo Kα) (mm^{-1})	1.809	2.290	2.574
T_{min} and T_{max}	0.7137, 0.7137	0.6573, 0.6573	0.7828, 0.6687
θ_{min} and θ_{max} (°)	3.08, 28.32	3.22, 29.37	2.75, 29.44
Number of total reflections	6149	8020	5878
Number of unique reflections (R_{int})	2414	2646	2750
Number of observed [$I \geqslant 2\sigma(I)$]	1876	2155	2236
Number of parameters	151	145	145
R_1/wR_2 [$I \geqslant 2\sigma(I)$]	0.0274, 0.0678	0.0267, 0.0705	0.0243, 0.0625
R_1/wR_2 (all data)	0.0410, 0.0716	0.0370, 0.0678	0.0356, 0.0651
GOF	1.040	1.102	1.109
$\Delta\rho$ (e/Å^3)	−0.369, 0.381	−0.355, 0.668	−0.407, 0.477

Infrared spectra were recorded by transmission through KBr pellets containing ca. 1% of the compounds using a Perkin–Elmer FTIR spectrum RX1.

UV–Vis absorption spectra were recorded by transmission through glycerol mulls of the grounded crystals held between two microscope slides by use of a UVIKON-XL of BIOTEK Instruments. For the cobalt compound a single crystal transmission spectrum was also measured. The crystal was mounted on cut slots between two aluminium sheets.

Thermogravimetric analyses were performed on approximately 40 mg of each sample using a Perkin–Elmer Pyris 6 TGA operating under dry nitrogen at a heating rate of 5 °C per minute.

Magnetic susceptibility measurements were performed in an applied field of 100 Oe on cooling from 300 to 2 K using a Quantum Design MPMS-5S SQUID magnetometer. Isothermal magnetizations at 2 K were measured for each compound from 0 to 50 kOe.

3. Results and discussion

3.1. Synthesis

The syntheses of crystals of $[NH_4][M^{II}(H_2O)(H_2PO_2)_3]$ for the three metals are quite dependent on the solvents, concentrations and other conditions as presented above. While acetone diffusion works well for manganese, it does not work for cobalt and nickel. Furthermore, the quality of crystals for cobalt is improved by addition of a bit of water while this procedure is not suitable for nickel. A wide range of conditions was tried and the optimised one for each metal is described above. We should note that using ethanol instead of methanol gives no crystals and using diffusion of acetone in pure aqueous solutions of the metal ions and $[NH_4][H_2PO_2]$ results in powders or crystals of another phase, $[M^{II}(H_2O)_6](H_2$-

$PO_2)_2$, where M = Co or Ni. It appears that different mixtures of methanol–water is required for every metals and the amount of water should be lower for the smaller cations, suggesting a subtle balance between solvation and complexation.

3.2. Structural characterization

The crystal structures of the three compounds, as determined from single crystals X-ray diffraction (Table 1), were found to be identical except for the bond distances and angles which vary in relation to the ionic radii of the metal cations (Table 2). The asymmetric unit (Fig. S1) contains one transition metal, three pyrophosphite (H_2PO_2), one water molecule and one ammonium cation. The key feature of the structures is the presence of one-dimensional chains of the transition metals with two bridging O–PH_2–O and terminal O–PH_2–O and H_2O to complete the octahedral coordination of the central metal (Figs. 1 and 2). One of the bridging O–PH_2–O coordinates adopts an *anti–anti* mode while the other adopts a *syn–anti* mode and the terminal O–PH_2–O is in an *anti*-coordination to the metals. A motif not observed in the chemistry of pyrophosphite coordination. The chains are parallel to one another and point along the 1 0 1 direction. Each chain is dipolar with the terminal O–PH_2–O groups pointing perpendicular to the chain axis and the water molecules point in the opposite direction. However, the chains are related by a 2_1 screw-axis so that neighbouring chains have their dipoles oppositely oriented. The bond distances are all normal with the average M–O increasing in the order Ni < Co < Mn while all the others are similar within experimental errors. The metal centres are only slightly distorted from octahedral geometry and the most noticeable is a 4+2 Jahn–Teller elongation where the longer bonds are to the uncoordinated O–PH_2–O. Within one chain the Jahn–Teller distortion alternates from site to site by nearly 90°. The bridging and terminal O–PH_2–O adopt almost identical geometry except for a slightly wider angle O–P–O of 119° for one of the bridging O–PH_2–O compared to 116° for the other two. Two important hydrogen bonds, involving the water molecule and the terminal O–PH_2–O, exist to connect the chains into a 3D-network. The first is between O7 (water) and O1 (the coordinated oxygen) and the second is between the O7 and O2 (the non-coordinated oxygen). The ammonium counter-balances the charge and sits in cavity.

Table 2
Bond lengths (Å) and angles (°) for $[NH_4][M^{II}(H_2O)(H_2PO_2)_3]$

	1	2	3
M(1)–O(5)	2.134(3)	2.0739(16)	2.0527(14)
M(1)–O(4)	2.157(2)	2.0914(15)	2.0546(13)
M(1)–O(3)	2.167(2)	2.0929(14)	2.0585(13)
M(1)–O(6)	2.185(2)	2.1102(15)	2.0738(13)
M(1)–O(7)	2.194(2)	2.0993(15)	2.0603(13)
M(1)–O(1)	2.202(2)	2.1244(14)	2.0786(12)
O(5)–M(1)–O(4)	93.08(9)	92.35(6)	92.36(5)
O(5)–M(1)–O(3)	176.84(10)	176.54(6)	176.40(6)
O(4)–M(1)–O(3)	86.60(8)	86.48(6)	86.54(5)
O(5)–M(1)–O(6)	88.17(10)	87.99(7)	87.38(6)
O(4)–M(1)–O(6)	93.68(9)	94.05(6)	93.68(5)
O(3)–M(1)–O(6)	88.71(8)	88.84(6)	89.27(5)
O(5)–M(1)–O(7)	91.69(10)	91.61(6)	91.53(6)
O(4)–M(1)–O(7)	173.55(9)	173.71(6)	173.76(6)
O(3)–M(1)–O(7)	88.88(9)	89.83(6)	89.87(5)
O(6)–M(1)–O(7)	90.81(9)	90.97(6)	91.38(5)
O(5)–M(1)–O(1)	95.12(10)	93.81(7)	93.60(6)
O(4)–M(1)–O(1)	88.65(9)	88.56(6)	88.93(5)
O(3)–M(1)–O(1)	88.02(8)	89.42(6)	89.81(5)
O(7)–M(1)–O(1)	86.60(9)	86.30(6)	85.95(5)
O(6)–M(1)–O(1)	175.87(9)	176.77(6)	177.18(5)

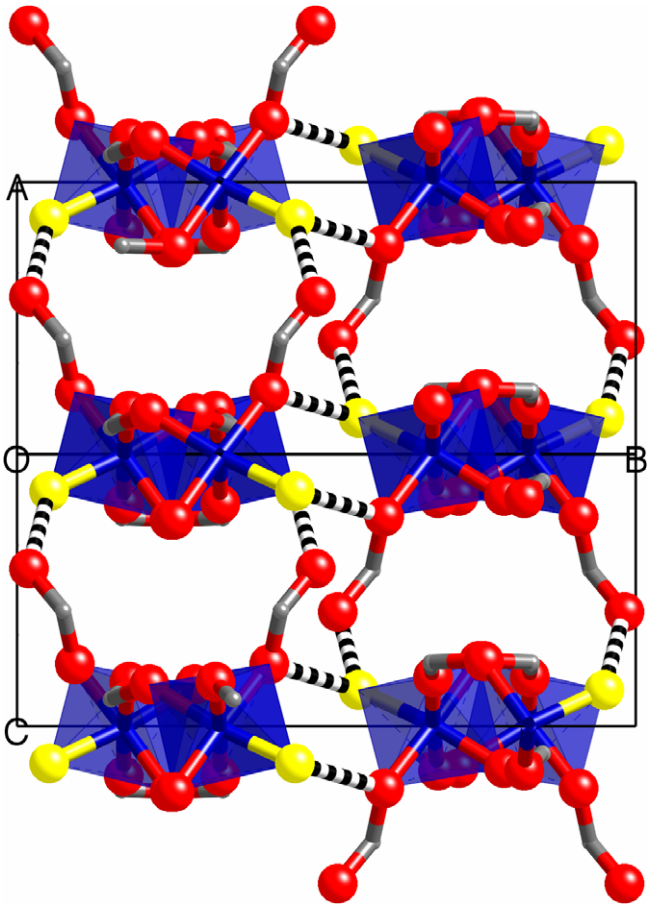

Fig. 1. Projection of the structure along the 1 0 1 direction showing the chains with the terminal O–PH_2–O pointing in opposite directions, and the hydrogen-bonds (black-white stripped) between the water (yellow) and the oxygen atoms of the terminal O–PH_2–O. (For interpretation of the references to colour in this figure legend, the reader is referred to the web version of this article.)

The single-crystal structure of $[Mn^{II}(H_2PO_2)_2(H_2O)]$ was also determined and found to correspond to that reported ($P2_1/c$, a = 7.8338(2), b = 7.3864(2), c = 10.7552(2) Å, β = 102.826(1)°, Z = 2, V = 606.81(3) Å^3 [16].

Although the HCO_2^- and $H_2PO_2^-$ have similar shape (not considering the hydrogen atoms), they have slightly different sizes and consequently, they show similar modes of coordination with the first row transition metals. Surprisingly, we have not found any isostructural coordination compound for the two ligands.

3.3. Powder X-ray diffraction

All the peaks in the powder diffraction patterns of the polycrystalline samples of the compounds (Fig. S2) were indexed to those calculated by RIETAN. This suggests there are no other crystalline phases present in the bulk samples within the experimental errors of ca. 1%. The diffraction pattern for **4** is also consistent with that determined from the single crystal structure (Figs. S3 and S4) [18].

3.4. Infrared spectroscopy

Infrared spectra of the three compounds are shown in Fig. 3 as well as those of the ammonium salt, **4** and **5** for comparison (Table 3). The spectra of the three compounds are almost identical to each other, confirming their isostructural nature. By comparison of the spectra to those of the ammonium salt, **4** and **5**, the NH_4, H_2O

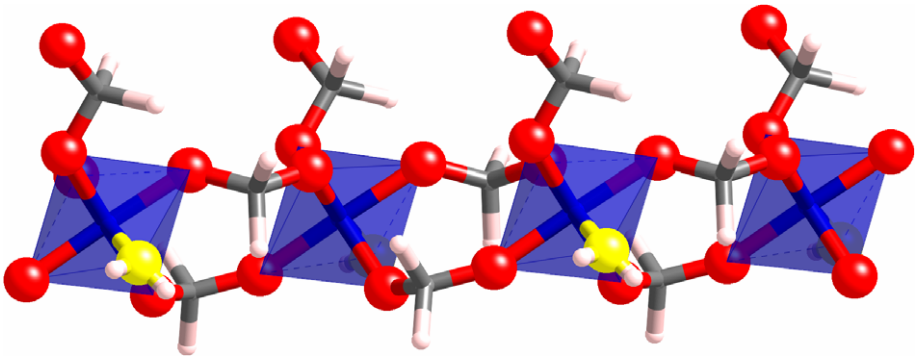

Fig. 2. Structure of a single chain showing the two bridging O–PH_2–O, the terminal O–PH_2–O and the water molecule (yellow). (For interpretation of the references to colour in this figure legend, the reader is referred to the web version of this article.)

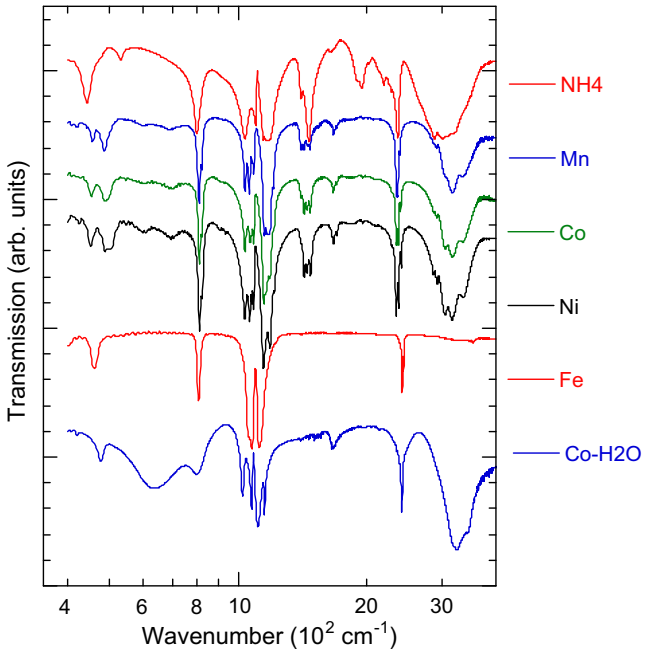

Fig. 3. Infrared transmission spectra of $[NH_4][(H_2PO_2)]$, **1**–**5** (from top to bottom).

and H_2PO_2 group frequencies can be identified [25]. The OH and NH stretching modes are observed above 3000 cm^{-1} and those of PH are in the range 2190–2400 cm^{-1}. The presence of three such peaks may be due to the three crystallographically independent O–PH_2–O groups. The bending modes of H_2O and NH_4 are seen at 1670 and 1400–1472 cm^{-1}, respectively, while those of PH_2 range between 1100 and 1175 cm^{-1}. The P-O modes are centred at 1075 cm^{-1}. A medium intensity peak at 810 cm^{-1} is assigned to the rocking mode of PH_2. The M–O bond stretch modes are weak and appear below 500 cm^{-1}.

3.5. UV-Vis spectroscopy

The UV–Vis absorption spectra of the complexes were recorded by transmission through suspensions of finely ground powders in glycerol held between two microscope slides (Fig. 4). The spectra therefore suffer from a high diffusion due to scattering which increases with energy. The absorption bands are superposed on this background. These spectra are limited to 350 nm due to absorption of the glycerol and the glass slides. In contrast the transmission spectra recorded through a masked single crystal are free of the high diffusion and are extended to the highest energy (180 nm). The spectrum for **2** shows two bands in the visible region; a strong one at 534 nm and a shoulder at 483 nm which are assigned to the $^4T_{1g}(F) \rightarrow {}^4T_{1g}(P)$ and $^4T_{1g}(F) \rightarrow {}^4A_{2g}$ transitions, respectively [26]. The strong bands in the UV region below 200 nm are possibly due to the ligands. The spectrum of **3** consists of two weak bands at 767 and 681 nm and a strong one at 417 nm. The former two are assigned to the $^3A_{2g} \rightarrow {}^3T_{1g}(F)$ which is split due to spin–orbit coupling that mixes the $^3T_{1g}$ and ^1E_g states. The band at 400 nm is the $^3A_{2g} \rightarrow {}^3T_{1g}(P)$ transition. For **1**, no band is observed in the visible. The observed spectra are characteristics of those of the corresponding divalent metals in an octahedral coordination of six oxygen atoms [26].

3.6. Thermogravimetric analyses

The results of the thermogravimetric analyses indicate that three isostructural compounds **1**, **2** and **3** behave slightly different (Fig. 5). They are stable up to 150 °C and the first weight loss corresponds to the departure of the coordinated water and it appears to be harder to remove for the nickel compound compared to those of cobalt and manganese. The second weight loss is the departure of NH_3. The remaining metal-phosphite has different stability for the three metals. Its stability increases from Mn to Ni and to Co. The products may be the results of different progression of condensation of H_2PO_2 to $H_4P_2O_3$, $H_6P_3O_4$ and higher weight oligomers.

The colourless crystals of **4** show stability to 200 °C followed by a weight loss amounting to the departure of two oxygen atoms and resulting in a light orange powder. The powder X-ray diffraction of the latter indicates that it is highly crystalline but TREOR and DICVOL are unable so far to find a unit cell. Two further steps to reach a mass corresponding to $FeH_6P_3O_4$.

3.7. Magnetic measurements

The magnetic susceptibilities and the inverse susceptibilities of the compounds are shown in Fig. 6. The results of the Curie–Weiss fit of the data and the temperature range are given in Table 4. Compounds **1**–**3** exhibit weakly antiferromagnetic coupling between nearest neighbours. The Curie constants are all normal for these cations in their divalent oxidation state. The Weiss temperature for the manganese complex is very small for a fit to the data covering the whole region of temperature and the lack of a maximum does not warrant further fitting of the data to a 1D-AF model. For **2**, the value is large due to the additional effect of spin-orbit coupling for this ion. In the case of **3**, the Weiss temperature is again low and it would require single-crystal measurements to separate the coupling strength from the single-ion anisotropy. The isothermal

Table 3
Frequencies and assignments of the bands in the spectra of the complexes [25]

1	2	3	4	5	$[NH_4][(H_2PO_2)]$	Assignment
3348 s, br	3350 s, br	3358 s, br		3440 s sh	3494 vw sh	ν(N–H)
3168 s, br	3156 s, br	3156 s, br		3242 vs	3220 s br	ν(O–H)
3052, sh	3048 s, br	3048 s, br		3177 vs	3080 s br	ν(O–H)
2908 vw	2912 vw	2918 vw			3004 s br	
2864 vw	2864 vw	2860 vw			2878 s br	
			2434 s			
			2416 s	2412 s		
2384 w	2398 w	2404 w			2356 s	ν(P–H)
2358 s	2364 s	2368 s			2282 vw	ν(P–H)
2350 s		2350 sh			2250 vw	ν(P–H)
2336 sh	2338 s	2338 s			2192 w	ν(P–H)
					2042 vw	
					1942 m	
					1896 vw	
	1698 vw	1700 vw				
1670 vw	1668 w	1670 w		1670 m	1634 vw	δ (H_2O)
1472 m	1472 m	1474 m			1462 s	δ (NH_2)
1450 m	1448 m	1446 m				δ (NH_2)
1424 m	1426 m	1426 m			1402 w	δ (NH_2)
1400 m	1402	1402 sh				δ (NH_2)
1210 sh	1212 sh	1214 vw				
1174 m	1184 m	1184 s			1178 s	δ (PH_2)
	1160 m			1152 s	1144 vw	δ (PH_2)
1148 m	1146 s	1144 s	1118 vs	1110 s		ν (PH_2)
1086 m	1086 m	1086 m				ν (PO_2)
1076 w	1074 sh	1074 m	1076 vs	1074 s		ν (PO_2)
1060 m	1064 m	1062 m	1055 s sh			ν (PO_2)
1036 m	1036 m	1036 m		1023 s	1036 s	ν (PO_2)
822 w	822 m	822 m				(PH_2) rock
810 m	812 m	812 m	807 s	800 s br	800 s	(PH_2) rock
				636 s br		
		502 w			530 vw	
486 w	488 w	488 w				
456 w	454 w	452 w	462 m	476 m	442 m	
				420 w		

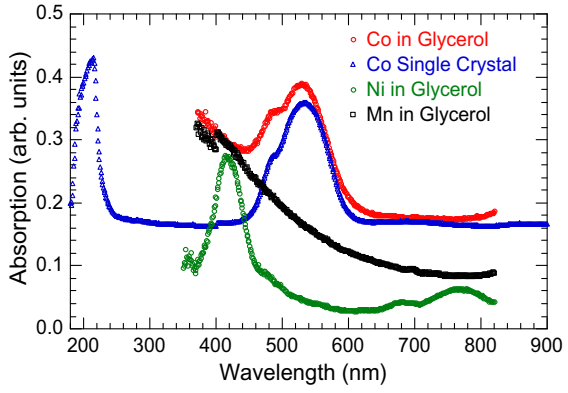

Fig. 4. Transmission UV–Vis spectra of **1**–**3**.

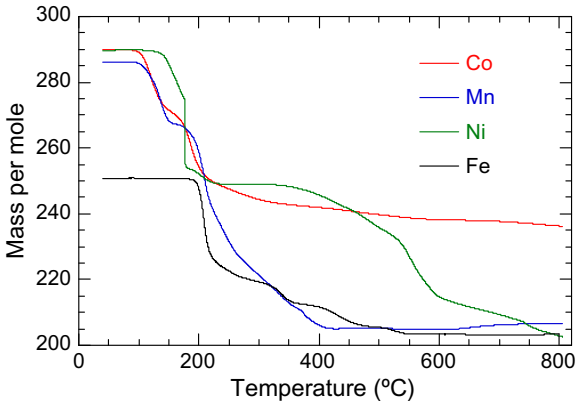

Fig. 5. Thermogravimetry for **1**–**4**.

magnetisations at 2 K also indicate the presence of AF coupling and therefore deviate from the Brillouin functions for the isolated paramagnets of spin 5/2, 3/2 and 1 (Fig. 7) [27].

The susceptibility of **4** is different to those of the divalent metals and it shows a maximum at 5 K (Fig. 8). The Curie–Weiss fit of the magnetic susceptibility of **4** for data above 50 K indicates antiferromagnetically coupled nearest neighbour interaction while a very good fit to a 1D-antiferromagnetic chain, using the equation below, is obtained for the whole temperature range with $2J/k$ of 1.20(1) K and g of 2.019(2) [28]. The slight deviation below 3 K may be due to the presence of interchain exchange interaction which appears to be also antiferromagnetic. Data at much lower temperatures will be needed to extract the interchain coupling energy. The isothermal magnetisation at 2 K also indicate the presence of AF coupling and exhibits a linear dependence on field without reaching saturation at the highest field of our SQUID magnetometer.

$$X = \left(\frac{Ng^2\mu_B^2 S(S+1)}{3kT}\right)\left(\frac{1+u}{1-u}\right)$$

$$u = \coth\left(\frac{2JS(S+1)}{kT}\right) - \left(\frac{kT}{2JS(S+1)}\right)$$

It is interesting to note that the coupling strength increases with the number of $H_{2PO_2}^{2-}$ bridges if we compare the two $S = 5$ ions, Mn^{II} and Fe^{III}, without taking into consideration of the ionic radii.

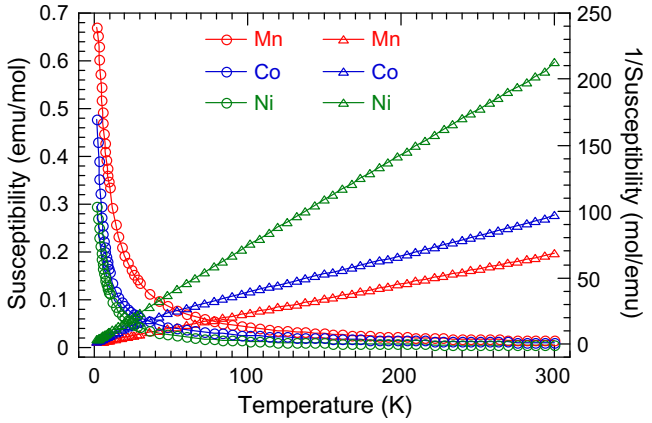

Fig. 6. Temperature dependence of the magnetic susceptibility (circles) and its inverse (triangles) for **1** (red), **2** (blue) and **3** (green). (For interpretation of the references to colour in this figure legend, the reader is referred to the web version of this article.)

Table 4
Summary of the magnetic parameters of the complexes.

	1	2	3	4
Temperature range (K)	2–294	100–294	2–300	50–294
C (cm^3 K mol^{-1})	4.464(2)	3.49(1)	1.428(2)	4.6(1)
θ (K)	−3.3(1)	−35.0(8)	−3.8(2)	−9.7(4)
1D AF-FIT				$2J/k$ = 1.20(1) K; g = 2.019(2)

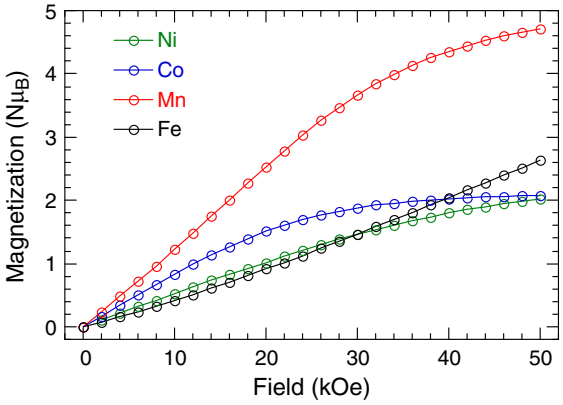

Fig. 7. Isothermal magnetisation for **1** (red), **2** (blue), **3** (green) and **4** (black). (For interpretation of the references to colour in this figure legend, the reader is referred to the web version of this article.)

However, these are still quite low energies. It is known for the 3D complexes containing formate bridges that the critical temperature of the magnetic transition is in the order Ni > Co ≈ Mn, which appears to be in the order of the ionic radii. For the present case no such relation can be drawn and therefore, more examples will be required to make comparison of the magnetic properties between those containing formate and pyrophosphite.

4. Conclusion

In the present work, we have isolated and characterised structurally and magnetically a novel series of transition metal one-dimensional polymers, $[NH_4][M^{II}(H_2O)(H_2PO_2)_3]$ where M = Mn, Co or Ni, having two bridging and one terminal O–PH_2–O groups.

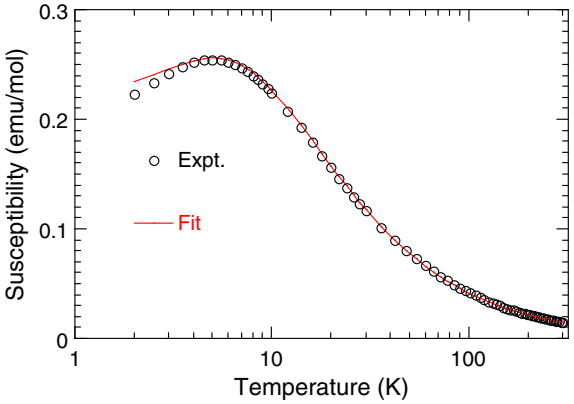

Fig. 8. Temperature dependence of the magnetic susceptibility of **4** (circles) and the fit to a 1D-AF model (solid line).

They all behave as Curie–Weiss paramagnets with weak antiferromagnetic near-neighbour interaction. In contrast, the polymer $[Fe^{III}(H_2PO_2)_3]$ with three bridging O–PH_2–O groups exhibits a one-dimensional antiferromagnetic behaviour.

Acknowledgements

We thank the CNRS and the University of Hiroshima for funding this work and Université Louis Pasteur for their hospitality to Y.Y. We are also grateful for the partial supports by a Grant-in-Aid for Science Research (A) (No. 18205023) and "Nanotechnology Support Project" of the Ministry of Education, Culture, Sports, Science, and Technology (MEXT), Japan.

Appendix A. Supplementary material

CCDC 419200, 419199, and 419198 contain the supplementary crystallographic data for this paper. These data can be obtained free of charge from The Cambridge Crystallographic Data Centre via www.ccdc.cam.ac.uk/data_request/cif. Numbering scheme adopted in the crystal structure determinations; the calculated and observed powder X-ray diffraction patterns of the complexes; the calculated and observed powder X-ray diffraction patterns of **4** and after its decomposition at 220 °C. Supplementary data associated with this article can be found, in the online version, at doi:10.1016/j.ica.2008.07.009.

References

[1] See the (a) 'Proceedings of the International Conference on Magnetism', J. Magn. Magn. Mater., 2007, 310(2);
(b) 'Proceedings of the International Symposium on Physics of Magnetic Materials', J. Magn. Magn. Mater., 2006, 303(2);
(c) 'Proceedings of the International Conference on Molecule-based Magnets (ICMM)', Polyhedron, 2003, 22(14–17); 2005, 24(6–17); 2007, 26(9–11).
[2] P. Day, A.E. Underhill (Eds.), Philos. Trans. Royal Soc. London, Ser. A 357 (1999) 1;
O. Kahn (Ed.), NATO ASI Ser., Ser. C (1996) 484;
K. Itoh, M. Kinoshita (Eds.), New Magn. Mater., Gordon Breach-Kodansha, Tokyo, 2000;
R.L. Carlin, Magneto-Chemistry, Springer-Verlag, Berlin, 1986.
(3) P.J. Hay, J.C. Thibeault, R. Hoffmann, J. Am. Chem. Soc. 97 (1975) 4884.
[4] S.J. Blundell, Magnetism in Condensed Matter, Oxford University Press, 2001; M.M. Schieber, Selected Topics in Solid State Physics, Experimental Magnetochemistry in: E.P. Wohlfarth (Ed.), vol. VIII, North-Holland, Amsterdam, 1967.
(5) X-Y. Wang, Z-M. Wang, S. Gao, Chem. Commun. (2007), doi:10.1039/b708122g.
[6] J. Ribas, A. Escuer, M. Monfort, R. Vicente, R. Cortés, L. Lezama, T. Rojo, Coord. Chem. Rev. 193–195 (1999) 1027.
(7) Y-Q. Tian, C.-X. Cai, X.-M. Ren, C.-Y. Duan, Y. Xu, S. Gao, X-Z. You, Chem. Eur. J. 9 (2003) 5673.

[8] M. Kurmoo, C.J. Kepert, New J. Chem. (1998) 1525;
S.R. Batten, K.S. Murray, Coord. Chem. Rev. 246 (2003) 103.
[9] A.S. Borovik-Romanov, N.M. Kreines, L.A. Prozorova, Zh. Éksp. Teor. Fiz., 45 (1963) 64. Sov. Phys. JETP, 1964, 18, 46;
A.S. Borovik-Romanov, V.G. Zhotikov, N.M. Kreines, Zh. Éksp. Teor. Fiz. 74 (1978) 2286. (Sov. Phys. JETP 1978, 47, 1188);
T. Lancaster, S.J. Blundell, F.L. Pratt, M. Kurmoo, Physica. B326 (2003) 522.
[10] M. Ohba, H. Okawa, Coord. Chem. Rev. 198 (2000) 313;
C.N.R. Rao, S. Natarajan, R. Vaidhyanathan, Angew. Chem., Int. Ed., 43 (2004) 1466.
[11] Z-M. Wang, B. Zhao, H. Fujiwara, H. Kobayashi, M. Kurmoo, Chem. Commun. (2004) 416;
Z.-M. Wang, B. Zhang, T. Otsuka, K. Inoue, H. Kobayashi, M. Kurmoo, Dalton Trans. (2004) 2209;
Z.-M. Wang, B. Zhang, M. Kurmoo, M.A. Green, H. Fujiwara, T. Otsuka, H. Kobayashi, Inorg. Chem. 44 (2005) 1230;
Z.-M. Wang, Y. Zhang, M. Kurmoo, T. Liu, S. Vilminot, B. Zhao, S. Gao, Aust. J. Chem. 59 (2006) 617;
Z.-M. Wang, B. Zhang, K. Inoue, H. Fujiwara, T. Otsuka, H. Kobayashi, M. Kurmoo, Inorg. Chem. 46 (2007) 437;
B. Zhang, Z-M. Wang, M. Kurmoo, S. Gao, K. Inoue, H. Kobayashi, Adv. Funct. Mater. 17 (2007) 577;
Z.-M. Wang, B. Zhang, Y.-J. Zhang, M. Kurmoo, T. Liu, S. Gao, H. Kobayashi, Polyhedron 26 (2007) 2207;
Z.-M. Wang, Y. Zhang, T. Liu, M. Kurmoo, S. Gao, Adv. Funct. Mater. 17 (2007) 1523;
Z.-M. Wang, X. Zhang, S.R. Batten, M. Kurmoo, S. Gao, Inorg. Chem. 46 (2007) 8439.
[12] M.I. Naumova, N.V. Kuratieva, D.Y. Naumov, N.V. Podberezskaya, J. Struct. Chem. 453 (2004) 465;
K.J. Gaskell, P.M.A. Sherwood, Surf. Sci. Spectra 9 (2004) 67.
[13] M.I. Naumova, N.V. Kuratieva, D.Y. Naumov, N.V. Podberezskaya, Acta Crystallogr. Sect. C 61 (2) (2005) i14;
C. Sugiura, A. Kamata, T. Kashiwakura, H. Tezuka, K. Suzuki, S.-I. Nakai, J. Phys. Soc. Jpn. 66 (1) (1997) 274;
N.V. Kuratieva, M.I. Naumova, D.Y. Naumov, N.V. Podberezskaya, J. Struct. Chem. 45 (2) (2004) 281.
[14] M.D. Marcos, P. Amoros, D. Beltran, A. Beltran, Powder Diffr. 9 (1) (1994) 15;
A. Le Bail, M.D. Marcos, P. Amoros, Inorg. Chem. 33 (12) (1994) 2607;
M.D. Marcos, P. Amoros, D. Beltran, A. Beltran, Inorg. Chem. 33 (6) (1994) 1220;
M.D. Marcos, R. Ibanez, P. Amoros, A. Le Bail, Acta Crystallogr., Sect. C 47 (6) (1991) 1152;
F. Sapina, P. Gomez-Romero, M.D. Marcos, P. Amoros, R. Ibanez, D. Beltran, R. Navarro, C. Rillo, F. Lera, Eur. J. Solid State Inorg. Chem. 26 (6) (1989) 603.
[15] M.D. Marcos, P. Amoros, F. Sapina, A. Beltran-Porter, R. Martinez-Manez, J.P. Attfield, Inorg. Chem. 32 (23) (1993) 5044;
M.D. Marcos, P. Amoros, A. Beltran, D. Beltran, Solid State Ionics 63–65 (1–4) (1993) 96;
S.A. Mikhalyuk, N.V. Romanova, Ukrainskii Khimicheskii Zhurnal (Russian Edition) 448 (1978) 803;
N.C. Johnson, W.E. Bull, Inorg. Chim. Acta 272 (1978) 191;
N.V. Kuratieva, M.I. Naumova, D.Y. Naumov, N.V. Podberezskaya, Acta Crystallogr., Sect. C 59 (1) (2003) i1;
G. Brun, M. Dumail, C.R. Acad. Sci. Ser. C 27223 (1971) 1866.
(16) M.D. Marcos, P. Amoros, F. Sapina, D.J. Beltran, Alloys Compd. 188 (1992) 133.
(17) D.Y. Naumov, M.I. Naumova, N.V. Kuratieva, E.V. Boldyreva, J.A.K. Howard, Acta Crystallogr. Sect. C 58 (5) (2002) i55.
[18] N.V. Kuratieva, D.Y. Naumov, Acta Crystallogr., Sect. C 62 (1) (2006) i9;
F. Mawrow, J. Zonew, Z. Anorg. Allg. Chem. 93 (1915) 311.
[19] J.A. Seddon, A.R.W. Jackson, R.A. Kresinski, A.W.G. Platt, Polyhedron 1511 (1996) 1899;
P.A. Tanner, S.T. Hung, T.C.W. Mak, R.J. Wang, Polyhedron 117 (1992) 817.
[20] D.Y. Naumov, M.I. Naumova, N.V. Podberezskaya, N.V. Kuratieva, Acta Crystallogr., Sect. C 60 (8) (2004) i73;
D.Y. Naumov, M.I. Naumova, N.V. Kuratieva, Acta Crystallogr., Sect.E 61 (11) (2005) i251.
[21] O.J. Parker, R.M. Harvey, G.L. Breneman, Acta Crystallogr. Sect. C 52 (4) (1996) 871;
D.Y. Naumov, D.S. Yufit, E.V. Boldyreva, J.A.K. Howard, Acta Crystallogr., Sect. C 57 (7) (2001) 790;
G.L. Breneman, M. Fields, O.J. Parker, Acta Crystallogr., Sect. E 58 (6) (2002) m262;
J. Sala-Pala, R. Kergoat, J.E. Guerchais, C.R. Acad. Sci. Ser. C 2746 (1972) 595.
(22) F. Izumi, T. Ikeda, Mater. Sci. Forum. 321–324 (2000) 198.
[23] G.M. Sheldrick, SADABS 2.05, University of Göttingen, Göttingen, Germany.
[24] G.M. Sheldrick, SHELX97 Programs for Crystal Structure Analysis, Tammanstrasse 4, D-3400 Gottingen, Germany, 1998;
SHELXTL 6.10; Bruker Analytical Instrumentation, Madison, WI, 2000.
[25] R.I. Bickley, H.G.M. Edwards, A. Knowles, J.K.F. Tait, R.E. Gustar, D. Mihara, S. Rose, J. Spectrochim. Acta Part A: Mol. Biomol. Spectrosc. 50A7 (1994) 1277;
R.I. Bickley, H.G.M. Edwards, R.E. Gustar, J.K.F. Tait, J. Mol. Struct. 273 (1992) 61;
P. Tanner, L. Yu-Long, T.C.W. Mak, Polyhedron 163 (1997) 495.
(26) A.B.P. Lever, Inorganic Electronic Spectroscopy, second ed., Elsevier, Amsterdam, 1984.
(27) A. Herpin, Theorie du Magnetisme, Presse Universitaire de France, Paris, 1968.
(28) M.E. Fisher, Am. J. Phys. 32 (1974) 241.